

Detailed investigation of the shearing mechanism of β'' precipitates in Al-Mg-Si alloys

Emil Christiansen^{1,2,*}, Calin Daniel Marioara³, Inga Gudem Ringdalen³, Ruben Bjørge³, Bjørn Holmedal^{1,4}, Odd Sture Hopperstad^{1,2}, and Randi Holmestad^{1,5}

¹Centre for Advanced Structural Analysis, NTNU – Norwegian University of Science and Technology — Norway.

²Department of Structural Engineering, Faculty of Engineering, NTNU – Norwegian University of Science and Technology — Norway.

³Materials and Nanotechnology, SINTEF Industry — Norway.

⁴Department of Materials Science and Engineering, Faculty of Natural Sciences, NTNU – Norwegian University of Science and Technology — Norway.

⁵Department of Physics, Faculty of Natural Sciences, NTNU – Norwegian University of Science and Technology — Norway.

Abstract. The mechanism behind shearing of β'' precipitates in Al-Mg-Si alloys during deformation is investigated by applying advanced transmission electron microscopy (TEM) techniques and frozen phonon multislice TEM image simulations on a selection of shearing configurations. In particular, the results indicate that the needle-like precipitates are sheared several times in single matrix Burgers vector steps. The multislice image simulations suggest that shearing events are most likely achieved in single Burgers vector steps, and there are some experimental evidence that the shearing planes are the matrix glide planes.

1 Introduction

During plastic deformation of precipitate strengthened alloys, dislocations either bypass or shear precipitates, depending on the precipitate phase, size, and shape [1]. In order to predict the strength of such alloys, it is important to understand the physical mechanisms of each process for various alloy systems and their precipitate phases.

The β'' precipitates are the main strengthening phase in the Al-Mg-Si alloy system (AA6xxx) and have composition $Mg_5Si_4Al_2$ [2]. They appear as long needles oriented along the matrix $\langle 100 \rangle$ and usually with a monoclinic unit cell with $a_{\beta''} = 15.16 \text{ \AA}$, $b_{\beta''} = 4.05 \text{ \AA}$, $c_{\beta''} = 6.74 \text{ \AA}$, and $\beta = 105.3^\circ$ with $(001) \parallel (010)_{\beta''}$, $[310] \parallel [001]_{\beta''}$, and $[\bar{2}30] \parallel [100]_{\beta''}$ [2–4]. Several studies indicate that these precipitates become sheared by gliding dislocations during deformation [5–9]. Because the precipitate crystal structure is different from the matrix structure, any matrix dislocation that glides through the precipitate phase will leave behind structural defects within and/or around the precipitate. The different matrix slip systems are not equivalent for a given precipitate and produce different results, depending on the slip system orientation to the precipitate. For instance, the geometrical shape of precipitate $(010)_{\beta''}$ cross-sections means that Burgers vectors with e.g. $[110]$ and $[\bar{1}\bar{1}0]$ will produce interface steps and internal planar defects of different surface areas. This illustrates the complexity of how these precipitates are sheared, as a glide of one particular Burgers vector through a precipitate will be different from other

Burgers vectors and produces different defects in the precipitate crystal structure. Hence, a variety in experimental results is to be expected, originating from the difference in crystal structures as discussed, but also due to a natural variation in precipitate shape, size, and experimental parameters such as thicknesses.

This study presents a combination of previously published experimental results (Christiansen *et al.* [9]) and recent frozen phonon multislice image simulation results. The results from the *post mortem* TEM experiments are explained and discussed in terms of the image simulation results. Together, the experimental and theoretical results indicate that β'' precipitates are sheared in single Burgers vector steps distributed along the needles. The results also form a basis for future works to better understand how this precipitate phase strengthens the industrially important AA6xxx alloys.

2 Materials and Methods

2.1 Materials

Cylindrical compression specimens, which measured 9 mm in diameter and 13 mm in height and were machined from an extruded AA6060 alloy with a composition given in table 1, were solution heat treated at 540 °C for 15 min in a salt bath, water quenched to room temperature, and left for 15 min to naturally age. They were then artificially aged to peak strength in an oil bath at 185 °C for 5 hours and air cooled to room temperature. The alloy has also been used in a number of studies investigating its

*e-mail: emil.christiansen@ntnu.no

Table 1. Nominal composition of AA6060 used in this study

	Fe	Si	Mg	Mn	Cr	Cu	Zn	Ti	Al
wt%	0.193	0.422	0.468	0.015	0.000	0.002	0.005	0.008	Bal
at%	0.093	0.406	0.520	0.007	0.000	0.001	0.002	0.005	Bal

crystallographic texture, grain size, and mechanical properties, and the reader is referred to these works for further details [10, 11]. The specimens were compressed to 20% engineering strain in an universal testing machine with a speed of 0.15 mm/min (strain rate of $2 \times 10^{-4} \text{ s}^{-1}$). Thin foils for TEM investigations were prepared from sections of the extrusion plane close to the middle of the compression specimens, please see Christiansen *et al* [12] for more details.

2.2 Methods

2.2.1 Microscopy

The experimental results presented in this paper are taken from an earlier study and are openly accessible through online repositories [9, 13].

Conventional bright field TEM, high resolution TEM (HRTEM), and scanning precession electron diffraction (SPED) experiments were conducted on a *JEOL JEM2100F* operated at 200 kV. HRTEM images were acquired on a *Gatan 2k UltraScan CCD*, while SPED data with a frame rate of 25 Hz was acquired by an external *Allied StingRay* CCD and the *NanoMEGAS DigiSTAR* system. For SPED, a precession angle of 1° and a precession frequency of 100 Hz were used, together with a nominal probe size of 1 nm and a step size of 1.52 nm. Virtual bright-field and dark-field images were produced from the SPED data and selected components from non-negative matrix factorisation (NMF) analysis were overlaid to show precipitate needles lying in-plane in order to investigate the shearing planes and their configuration (i.e. distribution along needle-lengths). The reader is referred to Christiansen *et al* [9] for more details.

Annular dark field scanning TEM (ADF STEM) data were acquired on a double-corrected *JEOL ARM200F* with a cold-FEG operated at 200 kV. *SmartAlign* was used to limit scan distortions in the data by acquiring 10–12 fast frames and by applying non-rigid image registration algorithms afterwards [14]. A collection semi-angle of 48–206 mrad and a probe convergence semi-angle of 27.42 mrad were used to acquire atomically resolved scans with a pixel dwell-time of 2 μs and pixel sizes $< 8 \text{ pm}$.

2.2.2 Image simulations

Frozen phonon multislice image simulations were performed using the *MULTEM* software package [15–17] with the parameters given in table 2. The simulation results presented in this paper are blurred with a Gaussian kernel of 1 \AA full width at half maximum to simulate the spatial incoherency of the electron source. The atomistic models used in the simulations were prepared using a combination of density functional theory, rigid translations,

and molecular dynamics. Virgin precipitate crystal structures were prepared by replicating a single β'' unit cell ($2 \times 100 \times 3$ unit cells) and inserting it into a matrix of aluminium ($20 \times 20 \times 100$ unit cells). The model thickness of 100 Al unit cells was chosen to match the average precipitate length in this alloy ($\sim 40 \text{ nm}$), although the specimen thicknesses in the experiments are $\sim 60 \text{ nm}$. The β'' unit cell was taken from density functional theory calculations [18]. The virgin precipitates were then rigidly sheared on various slip systems and with different configurations (various distribution of slip along the needle length). Due to limitations in both density functional theory and molecular dynamics, it is not possible to relax the sheared structures themselves, and this is an inherent limitation in the following multislice image simulations. The matrix, however, was relaxed using molecular dynamics in LAMMPS and using the Al-Mg potential by Liu and Adams to get realistic strain fields in the nearby matrix [19, 20]. The two precipitate models used to produce the multislice simulation results presented in this paper are shown in figure 1.

Table 2. Multislice simulation parameters

Parameter	Value	
Acceleration voltage	200 kV	
Detector response	homogeneous	
Potential sampling	$2048 \times 2048 \text{ pixels}^2$	
Model size	$80.64 \times 80.64 \text{ \AA}^2$	
Model thickness	403.2 \AA	
Slice thickness	2.025 \AA	
Temperature	300 K	
Phonon configurations	20	
	STEM	HRTEM
Convergence semi-angle	27mrad	–
Defocus C_1	0 nm	–57 nm
Spherical aberration C_3	–300 nm	1.0 mm
Inner collection semi-angle	48 mrad	–
Outer collection semi-angle	206 mrad	–
Image pixel size	0.162 \AA	0.039 \AA

3 Results and Discussion

3.1 SPED investigations

Figure 2 presents SPED results of precipitates in the virgin material and in 20% compressed specimens. The SPED technique produces a wealth of data, and advanced machine learning routines are needed to extract relevant and important data. In this figure, selected NMF components have been coloured and overlaid their corresponding virtual bright field images (i.e. each pixel value is determined by the diffracted intensity to a region containing the direct beam of that pixel's precession electron diffraction pattern). The virtual bright field images produce a rich contrast and dislocations appear as dark lines, while the NMF results show variation in scattering to in-plane β'' precipitate reflections. Due to the similarity of scattering angles of in-plane and out-of-plane needles, out-of-plane

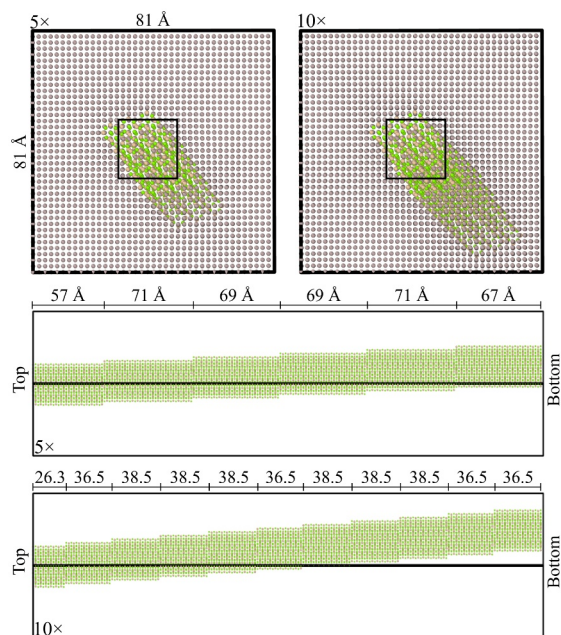


Figure 1. The two models used in the multislice simulations shown from the top and from the side with a [110] view (Al atoms removed). The regions scanned in the STEM simulations are shown as boxes in the middle of the top-views. Al, Mg, and Si atoms are shown in grey, green, and brown, respectively.

precipitates are also present in the NMF results and become coloured.

It is clear that the deformed specimen contains dislocations that are pinned by precipitates in the material. It is also clear that the NMF intensities (i.e. the brightness of the colour in figure 2) are irregular for the in-plane needles. This means that the scattering from these regions is different compared to the regions where the intensity is higher. While the bright regions of the in-plane needles scatter as expected, the darker regions scatter differently. It is, however, important to point out that the NMF results do not imply how the scattering is different, they only indicate that there is a difference.

Considering the single-pixel precession electron diffraction patterns of out-of-plane precipitates presented in figure 3, however, it becomes clear that certain precipitate reflections are suppressed after deformation. In turn, this must mean that the precipitate crystal structure is disrupted along their lengths. Together, these results show that deformation disrupts the precipitate structure in wide regions and that these regions seem to be distributed randomly along the needle lengths. The width of the dark regions is likely due to closely spaced and inclined shearing planes (with respect to the electron beam travelling along [001]). This will be further discussed in section 3.3.

3.2 High resolution results and simulations

There is a large variation in HRTEM and ADF STEM results from both virgin and deformed specimens, owing to the complex image forming mechanisms of the techniques.

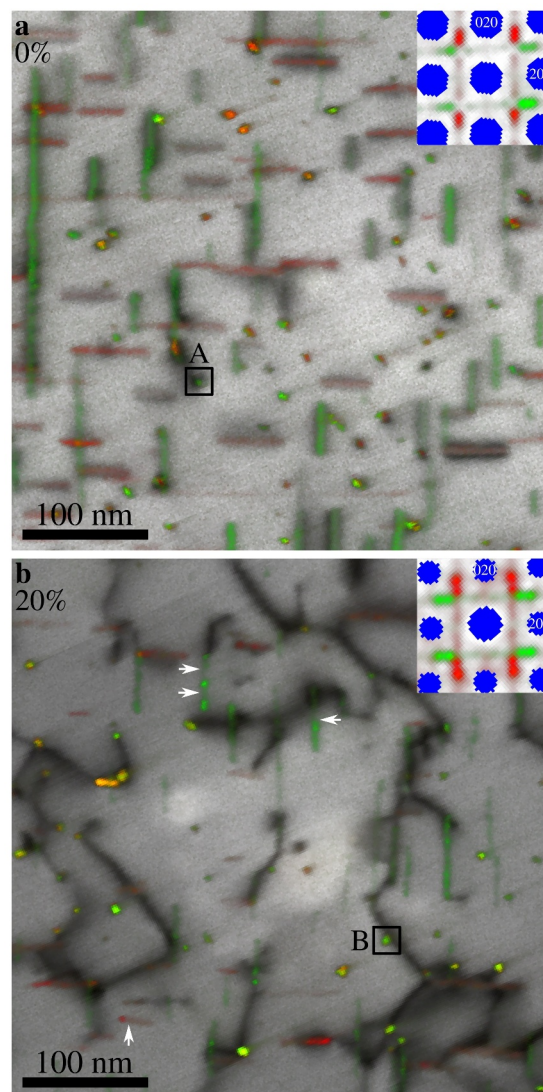


Figure 2. SPED results from virgin (a) and deformed (b) specimens. Red and green pixels scatter more significantly to red and green angles in the insets, respectively. Precipitates in deformed specimens contain dark regions (arrowheads) where scattering is reduced, indicating a disturbed crystal structure. The blue regions in the insets were not used in the NMF. Single-pixel precession electron diffraction patterns from out-of-plane precipitates marked A and B are shown in figure 3.

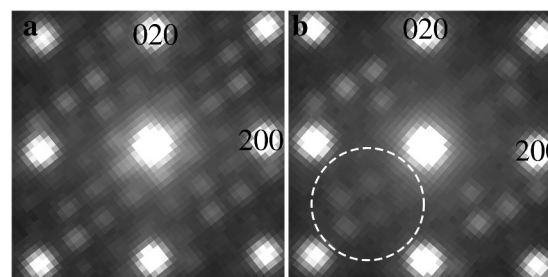


Figure 3. Single-pixel precession electron diffraction patterns from precipitates marked A (a) and B (b) in figure 2. Precipitates in deformed specimens tend to scatter less to certain reflections compared to precipitates in undeformed specimens.

In addition, the nature of the problem is also very complex, as each of the different twelve slip systems are different for the precipitate phase in addition to the possibility of glide on other planes, such as the (001) planes [21]. Hence, it is too ambitious to attempt to simulate and explain every experimental image. However, we have investigated shearing in a selection of different directions and planes with various distribution through the thickness of the model. There are three general trends. First, the influence of shearing plane (i.e. (001) versus (111)) on the appearance of simulated images is minimal. Second, different Burgers vectors produce different features in simulated images. In HRTEM, these features are most evident in the fast Fourier transforms (FFT) of the images, as different Burgers vectors alter the suppression of image Fourier components. For this paper, we focus on displacements of $\vec{b} = \vec{b}_{1\bar{1}0} = \frac{a}{2} [1\bar{1}0]$, as these capture the general trends of the features of both HRTEM and ADF STEM images. Third, distributed shearing events with an equal separation distance match better to experimental results than concentrated shearing events (i.e. either localised in a single plane producing one large step or localised in a narrow region producing many closely spaced single steps). Because there are many possible configurations, a full study of the influence of the through-thickness position of concentrated shearing events remains to be performed. In this paper, we consider results from models where the shearing events are distributed equally along the needle lengths, as this is a likely configuration with relatively few parameters.

3.2.1 Five shearing events

Figure 4 presents a comparison between selected experimental HRTEM and ADF STEM results in addition to simulated results for a precipitate that is sheared by $\vec{b} = \frac{a}{2} [1\bar{1}0]$ rigid translations on five equally spaced (001) planes through the thickness. β'' unit cells can be clearly seen in both the experimental and simulated ADF STEM results, which are almost indistinguishable from images of virgin materials (not shown). This can be explained by the sequential image forming mechanism of ADF STEM, where the first few nanometres of the specimen decide most of the final image. The precipitate imaged in HRTEM is also similar to the HRTEM simulation, although direct comparison is not possible due to the HRTEM image forming processes. Because contrast reversals and the thickness-sensitivity of HRTEM make it challenging to compare the images directly, the FFT power spectra of the images are better suited for comparison instead. Both the experimental HRTEM and the simulated HRTEM images produce FFT power spectra where certain Fourier components are suppressed, similar to the suppression of reflections in the precession electron diffraction patterns shown in figure 3.

While the experimental HRTEM and ADF STEM images are of different precipitates, these results reveal two important points. First, a precipitate that is sheared several times along its length may appear very similar to virgin precipitates in ADF STEM, but the HRTEM images

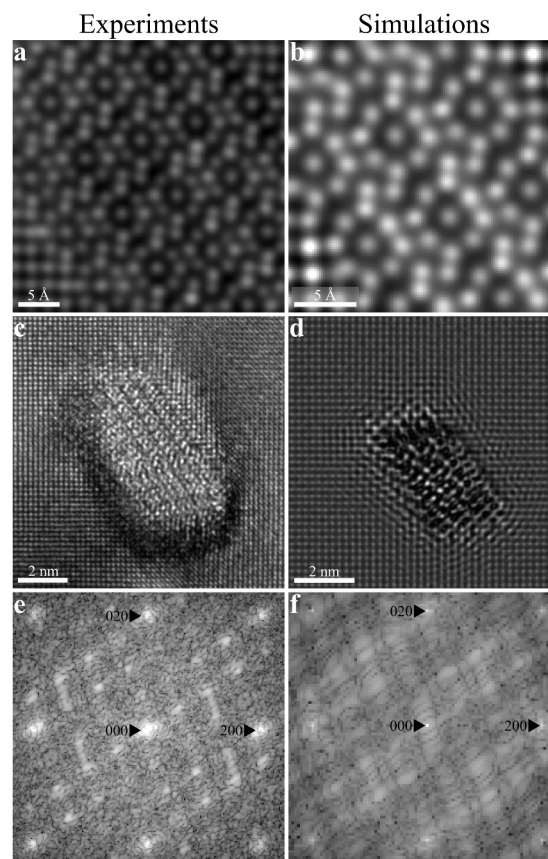


Figure 4. Comparison between experimental (a, c, e) results and multislice image simulation results from a model precipitate rigidly sheared 5 times along its length (b, d, f). ADF STEM results are shown in a and b, and HRTEM results are shown in c and d. FFT power spectra of the HRTEM images are given in e and f. Note that the experimental HRTEM and ADF STEM images are of different precipitates.

are greatly affected. This fits well with the large number of HRTEM images from deformed specimens that shows blurry precipitate cross-sections and FFT power spectra similar to the ones in figure 4e [13]. Second, precipitates that produce FFT power spectra such as the one given in figure 4e are likely sheared more than five times. Indeed, HRTEM image simulations of models with fewer number of shearing events reveal no noticeable suppression of Fourier components. Other Burgers vectors and shearing planes have also been tested, all indicating that 5 shearing events are needed to reproduce experimental HRTEM FFT power spectra.

3.2.2 Ten shearing events

Figure 4 presents experimental ADF STEM and HRTEM results and corresponding results from a multislice image simulation of a model with 10 shearing events distributed along the needle length. The shearing planes and directions are the same as for the simulations shown in figure 5. While the effect of more shearing events on the HRTEM simulation results is similar to the 5-shearing case (although more severe), the most clear changes appear in

the ADF results. With 10 shearing events, the ADF STEM results show a disrupted β'' atomic configuration instead of the more or less ideal β'' structure obtained from the 5-shearing case. The disruption resembles two β'' unit cells shifted by a single Burgers vector relative to each other, and follows the β'' unit cell periodicity. Inspecting the simulated ADF STEM images through the thickness (not shown), reveals that the disruption appears before the second shearing event and remains relatively unchanged as the beam progresses through the model. This clearly shows that it is not the number of shearing events that is of importance for the ADF STEM images, but their spacing and their distance to the specimen surface. On the other hand, the full through-thickness configuration is important for the HRTEM images, as the suppression of Fourier components becomes more severe when there are more shearing events.

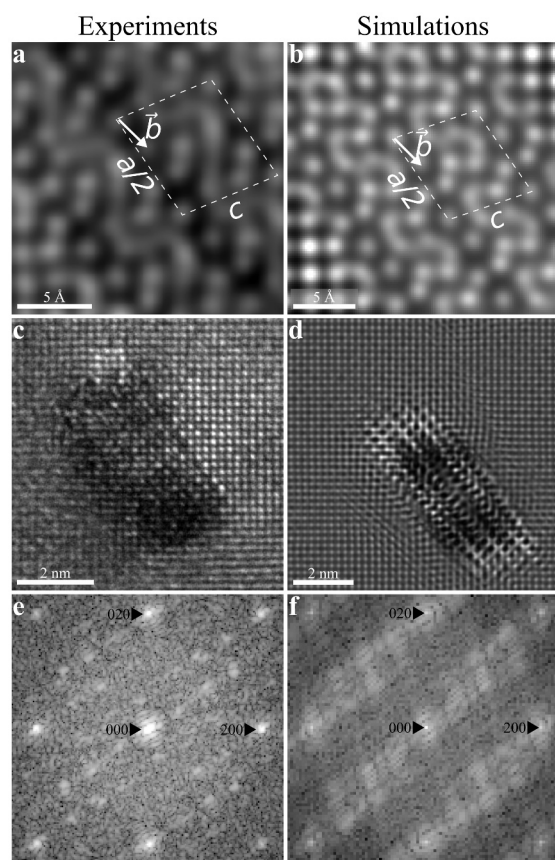


Figure 5. Comparison between experimental (a, c, e) results and multislice image simulation results from a model precipitate rigidly sheared 10 times along its length (b, d, f). ADF STEM results are shown in a and b, and HRTEM results are shown in c and d. FFT power spectra of the HRTEM images are given in e and f. Note that the experimental HRTEM and ADF STEM images are of different precipitates.

3.3 Deformation mechanisms

The β'' precipitates in the AA6060 alloy studied here are concluded to be sheared by dislocations during plastic de-

formation. In the following, the results are considered together to form a picture of likely deformation mechanisms.

When a β'' precipitate is sheared by a dislocation, the precipitate unit cells no longer match with each other across the shearing plane. This is evident from the different crystal structures, and is supported by SPED, HRTEM, and ADF STEM characterization. It is therefore reasonable to assume that atomic configurations close to the shear planes will shift and relax into new energy minima positions. Therefore, if the shearing plane itself is a planar defect, the effect of this defect will likely spread across nearby precipitate unit cells and disrupt the crystal structure locally. In turn, electron scattering from such regions will be altered and most likely reduced. We therefore suggest that the wide dark segments observed in SPED experiments are due to planar defects formed in the precipitates during deformation and their surrounding unit cell distortions. Given the relatively continuous contrast of the dark segments, we also suspect that the planar defects lie on planes inclined to the transverse direction of the needles (i.e. are not $(010)_{\beta''}$ planes).

For HRTEM images to develop the experimentally observed suppression of Fourier components, a number of shearing events must have taken place. At the same time, each of these shearing events must be spaced far enough apart for the electron beam to develop a marked phase shift. Considering the ADF STEM image in figure 5a, in which the precipitate has likely been sheared by a single dislocation close to the specimen surface (and possibly more times through its full thickness), it seems reasonable to conclude that shearing of β'' precipitates is achieved in single Burgers vector steps, and that these shearing events are spaced at least a few unit cells apart. If the shearing planes were spaced relatively far apart, the probability of having a shearing plane close to the specimen surface would be very low. Even though ADF STEM is not a statistical tool we have at least one image where this seems to be the case. In principle, it is also possible that the steps are some integer multiple of the matrix Burgers vector, rather than a single Burgers vector. However, this will require relatively large local plastic strains in order to achieve the number of planar defects that fits the SPED and HRTEM observations. Hence, it is likely that β'' precipitates are sheared in single Burgers vector steps on planes spaced a few nano meters apart. In some cases, dislocations may localise into narrow slip bands for a number of reasons, and this will then make the shearing planes more concentrated.

So far, we have not investigated the effect of combining different slip systems and other realistic shearing configurations, such as several bands of narrowly spaced shearing events using multislice image simulations. Such investigations would be useful to further understand the deformation mechanisms of β'' precipitates. In addition, the sheared precipitates were modelled as rigid translations of a perfect β'' needle, while we suspect that the planar defects distort the crystal lattice in their vicinity as well. Once more advanced atomic interaction potentials for molecular dynamics simulations are available, such effects could also be studied. For future work, we would

suggest imaging the same precipitate in ADF STEM and HRTEM and to compare the images with detailed multislice image simulations.

4 Conclusions

Three advanced and complementary TEM techniques show that β'' precipitates in the AA6060 alloy are sheared by dislocations during deformation. Multislice image simulations aid the interpretation of the experimental results and show that several closely spaced shearing planes produce images similar to the experimental data. In terms of deformation mechanisms, we propose that β'' precipitates are sheared in several and equally spaced single Burgers vector steps on {111} planes.

Acknowledgements

This work was funded by the Research Council of Norway through SFI CASA (grant number 237885), NORTEM (grant number 197405), and Mind The Gap (231762). The simulations were carried out on the EPIC [22] infrastructure at the IDUN cluster at the NTNU HPC Group, while the atomistic models were created using the Sigma2 HPC clusters (grant numbers 269905/NN9158K).

References

- [1] A. J. Ardell, Metallurgical Transactions A **16**, 2131–2165 (1985)
- [2] T. Saito, E. A. Mørtzell, S. Wenner, C. D. Marioara, S. J. Andersen, J. Friis, K. Matsuda & R. Holmestad, Advanced Engineering Materials **20**, 1800125 (2018)
- [3] G.A. Edwards, K. Stiller, G. L. Dunlop & M. J. Couper, Acta Materialia **46**, 3893–3904 (1998)
- [4] S. J. Andersen, H. W. Zandbergen, J. Jansen, C. Træholt, U. Tundal & O. Reiso, Acta Materialia **46**, 3283–3298 (1998)
- [5] F. Delmas, M. Vivas, P. Lours, M. J. Casanove, A. Couret & A. Coujou, Materials Science and Engineering A **340**, 286–291 (2003)
- [6] W. J. Poole, X. Wang, D. J. Lloyd & J. D. Embury, Philosophical Magazine **85**, 3113–3135 (2005)
- [7] K. Misumi, K. Kaneko, T. Nishiyama, T. Maeda, K. Yamada, K. Ikeda, M. Kikuchi, K. Takata, M. Saga & K. Ushioda, Journal of Alloys and Compounds **600**, 29–33 (2014)
- [8] Ø. Ryen, B. Holmedal, K. Marthinsen & T. Furu, Materials Science and Engineering **89**, 012013 (2015)
- [9] E. Christiansen, C. D. Marioara, B. Holmedal, O. S. Hopperstad, R. Holmestad, Scientific Reports **9**, 17446 (2019)
- [10] M. Khadyko, S. Dumoulin, T. Børvik & O. S. Hopperstad, International Journal of Mechanical Sciences **88**, 25–36 (2014)
- [11] B. H. Frodal, L. E. Dæhli, T. Børvik, O. S. Hopperstad, International Journal of Plasticity **188**, 36–69 (2019)
- [12] E. Christiansen, C. D. Marioara, K. Marthinsen, O. S. Hopperstad, R. Holmestad, Materials Characterization **144**, 522–531 (2018)
- [13] E. Christiansen, C. D. Marioara, B. Holmedal, O. S. Hopperstad & R. Holmestad, *Data for "Nano-scale characterisation of sheared β'' precipitates in a deformed Al-Mg-Si alloy"*, Dataset Version 1 archived in Zenodo, DOI: 10.5281/zenodo.2652906 (2019)
- [14] L. Jones, H. Yang, T. J. Pennycook, M. S. J. Marshall, S. Van Aert, N. D. Browning, M. R. Castell & P. D. Nellist, Advanced Structural and Chemical Imaging **1**, 8 (2015)
- [15] I. Lobato & D. Van Dyck, Ultramicroscopy **156**, 9–17 (2015)
- [16] I. Lobato, S. Van Aert & J. Verbeeck, Ultramicroscopy **168**, 17–27 (2016)
- [17] MULTEM, <https://github.com/Ivanlh20/MULTEM>
- [18] P. H. Ninive, A. Strandlie, S. Guldbrandsen-Dahl, W. Lefebvre, C. D. Marioara, S. J. Andersen, J. Friis, R. Holmestad & O. M. Løvvik, Acta Materialia **69**, 126–134 (2014)
- [19] S. Plimpton, Journal of Computational Physics **117**, 1–19 (1995)
- [20] X. -Y. Liu & J. Adams, Acta Materialia **46**, 3467–3476 (1998)
- [21] F. Delmas, J. Majimel, M. Vivas, G. Molenat, A. Couret & A. Coujou, Philosophical Magazine Letters **83**, 289–296 (2003).
- [22] M. Själander, M. Jahre, G. Tufte, N. Reissmann, *EPIC: An Energy-Efficient, High-Performance GPGPU Computing Research Infrastructure*, arXiv: 1912.05848.